Analysis of SARS-CoV-2 infection dynamic in vivo using reporter-expressing viruses

Chengjin Ye[a,b,1], Kevin Chiem[a,b], Jun-Gyu Park[a,b], Jesus A. Silvas[a,b], Desarey Morales Vasquez[a,b], Julien Sourimant[c], Michelle J. Lin[d], Alexander L. Greninger[d], Richard K. Plemper[c], Jordi B. Torrelles[a,b], James J. Kobie[e], Mark R. Walter[f], Juan Carlos de la Torre[g], and Luis Martinez-Sobrido[a,b,1]

[a]Host-Pathogen Interactions Program, Texas Biomedical Research Institute, San Antonio, TX 78227; [b]Population Health Program, Texas Biomedical Research Institute, San Antonio, TX 78227; [c]Center for Translational Antiviral Research, Institute for Biomedical Sciences, Georgia State University, Atlanta, GA 30303; [d]Virology Division, Department of Laboratory Medicine, University of Washington, Seattle, WA 98195; [e]Department of Medicine, Division of Infectious Diseases, University of Alabama at Birmingham, Birmingham, AL 35294; [f]Department of Microbiology, University of Alabama at Birmingham, Birmingham, AL 35294; and [g]Department of Immunology and Microbiology, The Scripps Research Institute, La Jolla, CA 92037

Edited by Xiang-Jin Meng, Virginia Polytechnic Institute and State University, Blacksburg, VA, and approved August 5, 2021 (received for review June 23, 2021)

Severe acute respiratory syndrome coronavirus 2 (SARS-CoV-2), the causative agent of the current COVID-19 pandemic, is one of the biggest threats to public health. However, the dynamic of SARS-CoV-2 infection remains poorly understood. Replication-competent recombinant viruses expressing reporter genes provide valuable tools to investigate viral infection. Low levels of reporter gene expressed from previous reporter-expressing recombinant (r)SARS-CoV-2 in the locus of the open reading frame (ORF)7a protein have jeopardized their use to monitor the dynamic of SARS-CoV-2 infection in vitro or in vivo. Here, we report an alternative strategy where reporter genes were placed upstream of the highly expressed viral nucleocapsid (N) gene followed by a porcine tescherovirus (PTV-1) 2A proteolytic cleavage site. The higher levels of reporter expression using this strategy resulted in efficient visualization of rSARS-CoV-2 in infected cultured cells and excised lungs or whole organism of infected K18 human angiotensin converting enzyme 2 (hACE2) transgenic mice. Importantly, real-time viral infection was readily tracked using a noninvasive in vivo imaging system and allowed us to rapidly identify antibodies which are able to neutralize SARS-CoV-2 infection in vivo. Notably, these reporter-expressing rSARS-CoV-2, in which a viral gene was not deleted, not only retained wild-type (WT) virus-like pathogenicity in vivo but also exhibited high stability in vitro and in vivo, supporting their use to investigate viral infection, dissemination, pathogenesis, and therapeutic interventions for the treatment of SARS-CoV-2 in vivo.

COVID-19 | SARS-CoV-2 | in vivo imaging | reporter viruses

Coronaviruses (CoVs) are enveloped, single-stranded, positive-sense RNA viruses that belong to the *Coronaviridae* family that can cause mild to severe respiratory infections in humans (1). Two CoVs have been associated with severe respiratory syndrome in the past two decades: severe acute respiratory syndrome CoV (SARS-CoV) in 2002–2003 and Middle East respiratory syndrome CoV (MERS-CoV) in 2012 to the present (2). Severe acute respiratory syndrome coronavirus 2 (SARS-CoV-2) emerged in the Chinese city of Wuhan in December 2019 and is the causative agent of the COVID-19 pandemic (3, 4). As of June 2021, SARS-CoV-2 has been reported to be responsible for over 150 million human infection cases and more than 3 million deaths around the World (https://covid19.who.int/).

Like SARS-CoV and MERS-CoV, SARS-CoV-2 mainly replicates in the upper (nasal turbinate) and lower (lungs) respiratory tract, resulting, in some cases, in fatal respiratory illness (5, 6). However, the intrahost dissemination and pathogenesis of SARS-CoV-2 are not well understood. Several animal models of SARS-CoV-2 infection have been established and have already provided very valuable information to understand the mechanism of tissue and cell tropism, replication, and pathogenesis (7–11). However, assessing the presence of SARS-CoV-2 in infected animals, organs, or tissues has required collection and processing of samples upon euthanasia, which complicates studies examining the longitudinal dynamic of a viral infection within an infected host. Recombinant (r)SARS-CoV-2 expressing reporter genes could overcome this problem and allow tracking of viral infection in vivo and in real time by monitoring the expression of the reporter gene. We and others have documented the feasibility of generating reporter-expressing rSARS-CoV-2 using a reverse genetic system (12, 13). These rSARS-CoV-2 have been genetically engineered to express the reporter gene by substituting the viral open reading frame (ORF) 7a protein with the reporter gene of interest, an experimental approach first employed to generate reporter-expressing rSARS-CoV (14). Despite these reporter-expressing rSARS-CoV-2 showing plaque phenotype, replication, and growth kinetics comparable to those of wild-type virus (rSARS-CoV-2/WT) in vitro (12, 13, 15), it is unclear whether the reporter-expressing rSARS-CoV-2 lacking ORF7a recapitulate viral pathogenicity in vivo and whether reporter gene expression levels could be efficiently tracked ex vivo using tissues or organs from infected animals, or in a whole organism in vivo.

In this study, we cloned fluorescent (Venus) and luciferase (Nano luciferase, Nluc) reporter genes upstream of the SARS-CoV-2

Significance

To date, due to the insufficient expression level of reporter genes from previous recombinant (r)SARS-CoV-2, in which the viral open reading frame (ORF) 7a gene was replaced by reporter genes, tracking the SARS-CoV-2 infection dynamic has been challenging. Here, we engineered rSARS-CoV-2 expressing fluorescent (Venus) or luciferase (Nano luciferase) reporter genes from the viral nucleocapsid (N) locus, without deleting any viral gene. These novel reporter-expressing rSARS-CoV-2, which give a higher expression level of reporter genes, allow us to monitor SARS-CoV-2 replication dynamic both in vitro and in vivo. These new reporter-expressing rSARS-CoVs-2 represent an excellent option to assess viral replication, tropisms, and pathogenicity as well as the rapid in vivo evaluation of effective countermeasures for the treatment of SARS-CoV-2 infection.

Author contributions: L.M.-S. designed research; C.Y., K.C., J.-G.P., J.A.S., and D.M.V. performed research; J.S., M.J.L., A.L.G., R.K.P., J.B.T., J.J.K., M.R.W., J.C.d.l.T., and L.M.-S. contributed new reagents/analytic tools; C.Y., K.C., J.-G.P., J.A.S., J.S., M.J.L., A.L.G., R.K.P., J.B.T., J.J.K., M.R.W., J.C.d.l.T., and L.M.-S. analyzed data; and C.Y. and L.M.-S. wrote the paper.

Competing interest statement: J.-G.P., J.J.K., M.R.W., and L.M.-S. are coinventors on a patent that includes claims related to some of the NAbs described.

This article is a PNAS Direct Submission.

[1]To whom correspondence may be addressed. Email: cye@txbiomed.org or lmartinez@txbiomed.org.

Published September 24, 2021.

nucleocapsid (N) gene separated by the porcine tescherovirus (PTV-1) 2A proteolytic cleavage site to generate new reporter-expressing rSARS-CoV-2 without the deletion of the ORF7a protein. In vitro, rSARS-CoV-2 expressing reporter genes from the viral N locus replicated and made viral plaques similar to those of rSARS-CoV-2/WT. Reporter-expressing rSARS-CoV-2 generated using this 2A strategy expressed higher levels of reporter gene expression compared to those rSARS-CoV-2 generated by substituting the viral ORF7a protein with the reporter gene of interest. Importantly, rSARS-CoV-2/Venus-2A and rSARS-CoV-2/Nluc-2A showed rSARS-CoV-2/WT–like pathogenicity in vivo. The higher level of Venus expression from rSARS-CoV-2/Venus-2A allowed us to detect viral infection in the lungs of infected K18 human angiotensin converting enzyme 2 (hACE2) transgenic mice using an in vivo imaging system (IVIS). Moreover, Venus expression from rSARS-CoV-2/Venus-2A was stable up to seven passages in vitro in cultured Vero E6 cells and in vivo up to day 6 postinfection. Importantly, levels of Venus expression correlated well with viral titers detected in the lungs, demonstrating the feasibility of using Venus expression as a valid surrogate marker to evaluate SARS-CoV-2 infection. Using rSARS-CoV-2/Nluc-2A, we were able to track the dynamic of viral infection in real time and longitudinally assess SARS-CoV-2 infection in vivo. Finally, we testified to the feasibility of using the rSARS-CoV-2/Nluc-2A to rapidly and accurately identify antibodies that neutralize viral infection in vivo.

Our data demonstrate that these next-generation rSARS-CoV-2 expressing reporter genes we have generated can be used to easily monitor viral infection in cultured cells and in validated animal models of infection. Importantly, our new rSARS-CoV-2/Venus-2A or rSARS-CoV-2/Nluc-2A retain similar virulence to that of rSARS-CoV-2/WT in K18 hACE2 transgenic mice and can be used to investigate viral replication, tropism, and viral dissemination and pathogenesis in vivo and to rapidly identify therapeutics for the treatment of SARS-CoV-2 infection and associated COVID-19 disease.

Results

Generation of rSARS-CoV-2 Expressing Venus. We have recently described the generation and characterization of rSARS-CoV-2 where a reporter gene of interest replaced the viral ORF7a protein (13). However, these rSARS-CoV-2 showed low levels of reporter gene expression during viral infection. To increase expression levels of reporter gene during SARS-CoV-2 infection and avoid the deletion of ORF7a protein, we implemented a strategy we previously used to generate recombinant influenza viruses and mammarenaviruses (16, 17). In this approach, the sequences of the reporter Venus fluorescent protein and the porcine teschovirus 1 (PTV-1) 2A self-cleaving peptide (18) were cloned upstream of the SARS-CoV-2 N gene (Fig. 1*A*), and the sequences harboring the fusion Venus-2A-N were cloned into the previously described bacterial artificial chromosome (BAC) containing the entire SARS-CoV-2 genome (19, 20). We rescued rSARS-CoV-2/Venus-2A virus according to our previously described protocol (19, 20). Vero E6 cells infected with the tissue culture supernatant (TCS) from Vero E6 cells transfected with the BAC containing the viral genome of rSARS-CoV-2/Venus-2A resulted in the expression of Venus in the same cells expressing the viral N protein (Fig. 1*B*). Venus was readily detected in whole cell lysate from rSARS-CoV-2/Venus-2A–, but not rSARS-CoV-2/WT–infected Vero E6 cells, while the viral N protein was detected in lysate obtained from both rSARS-CoV-2/Venus-2A– and rSARS-CoV-2/WT–infected Vero E6 cells (Fig. 1*C*). We confirmed the genetic identity of rSARS-CoV-2/Venus-2A using RT-PCR to amplify the Venus sequence and the entire sequence between ORF8 and N. The Venus fragment was amplified from cells infected with rSARS-CoV-2/Venus-2A, while the fragment between ORF8 and N was detected in cells infected with either rSARS-CoV-2/WT or rSARS-CoV-2/Venus-2A. As predicted, the amplified fragment from rSARS-CoV-2/Venus-2A–infected cells had a higher molecular size than the one obtained from rSARS-CoV-2/WT–infected cells (Fig. 1*D*).

In Vitro Characterization of rSARS-CoV-2/Venus-2A. We next assessed the fitness of rSARS-CoV-2/Venus-2A in Vero E6 cells by evaluating its growth kinetics, plaque phenotype, and reporter expression and compared them to our previously described rSARS-CoV-2/Δ7a-Venus and rSARS-CoV-2/WT. The rSARS-CoV-2/Venus-2A showed similar growth kinetics to those of rSARS-CoV-2/WT or rSARS-CoV-2/Δ7a-Venus (Fig. 2*A*). Likewise, rSARS-CoV-2/Venus-2A, rSARS-CoV-2/WT, and rSARS-CoV-2/Δ7a-Venus exhibited similar plaque phenotypes (Fig. 2*B*). Notably, plaques formed by rSARS-CoV-2/Venus-2A, but not those of rSARS-CoV-2/Δ7a-Venus, could be readily detected using a fluorescent imaging system, most likely because of the higher levels of Venus expressed from the locus of the viral N than those from the locus of the viral ORF7a (Fig. 2*B*). We next examined Venus expression in Vero E6 cells infected (MOI [multiplicity of infection] 0.001) with either rSARS-CoV-2/Venus-2A or rSARS-CoV-2/Δ7a-Venus. Both infections showed peak Venus expression at 48 h postinfection (hpi), but Venus expression levels from rSARS-CoV-2/Venus-2A–infected Vero E6 cells were higher than those infected with rSARS-CoV-2/Δ7a-Venus (Fig. 2*C*). To confirm this, we prepared whole cell lysates from mock, rSARS-CoV-2/Venus-2A–, and rSARS-CoV-2/Δ7a-Venus–infected Vero E6 cells and analyzed them by Western blot. Venus expression levels in rSARS-CoV-2/Venus-2A–infected Vero E6 cells were greater than those of rSARS-CoV-2/Δ7a-Venus–infected cells at all time points, whereas expression levels of N protein were comparable at all time points in Vero E6 cells infected with rSARS-CoV-2/Venus-2A and rSARS-CoV-2/Δ7a-Venus (Fig. 2*D*).

In Vivo Characterization of rSARS-CoV-2/Venus-2A. K18 transgenic mice expressing hACE2 have been shown to be a good animal model of SARS-CoV-2 infection (8, 21). We therefore examined whether SARS-CoV-2 infection could be tracked ex vivo using Venus expression. To that end, K18 hACE2 transgenic mice were infected intranasally with 10^5 plaque-forming units (pfu) of rSARS-CoV-2/Venus-2A, rSARS-CoV-2/Δ7a-Venus, or rSARS-CoV-2/WT (Fig. 3). Mice were killed at 1, 2, 4, and 6 d postinfection (dpi), and their lungs were excised and imaged ex vivo using an IVIS (AMI spectrum). Venus expression was readily detected in all lungs obtained from mice infected with rSARS-CoV-2/Venus-2A but not from those infected with rSARS-CoV-2/Δ7a-Venus or rSARS-CoV-2/WT (Fig. 3*A*). Quantitative analyses showed that Venus intensity peaks at 2 dpi and decreases over the course of infection in the lungs of infected mice (Fig. 3*B*). Nevertheless, gross lesions on the lung surface of mice infected with rSARS-CoV-2/Venus-2A were comparable to those observed in rSARS-CoV-2/WT– or rSARS-CoV-2/Δ7a-Venus–infected mice (Fig. 3 *C* and *D*). In addition, infection with rSARS-CoV-2/Venus-2A and rSARS-CoV-2/Δ7a-Venus resulted in comparable viral titers to those observed in K18 hACE2 transgenic mice infected with rASRS-CoV-2/WT in all organs at all times pi (Fig. 3*E*), suggesting that the undetectable Venus expression in the lungs of K18 hACE2 mice infected with rSARS-CoV-2/Δ7a-Venus is unlikely due to lower levels of viral replication in vivo. Notably, we observed a correlation between virus replication and fluorescence intensity in the lungs (Fig. 3*F*).

To investigate the pathogenicity of rSARS-CoV-2/Venus-2A, we infected (10^5 pfu) K18 hACE2 transgenic mice intranasally with rSARS-CoV-2/Venus-2A, rSARS-CoV-2/Δ7a-Venus, or rSARS-CoV-2/WT, and monitored changes in body weight and survival rate for 12 d after viral infection. All infected mice showed significant body weight loss starting from 4 dpi (Fig. 3*G*).

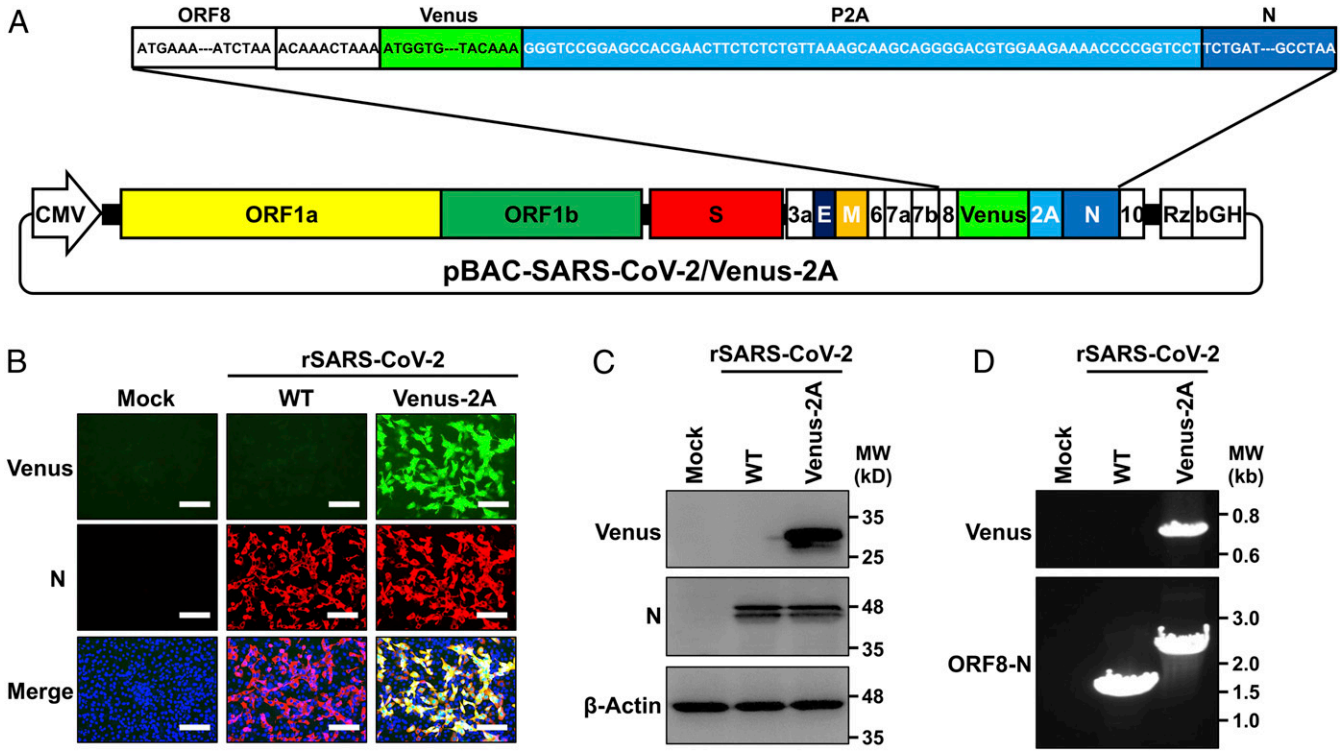

Fig. 1. Generation of an rSARS-CoV-2 expressing Venus-2A. (*A*) Schematic representation of the BAC for generation of rSARS-CoV-2/Venus-2A. The sequence encoding the fusion construct Venus-2A was inserted in the viral genome of SARS-CoV-2 in the BAC. The viral ORF8, the intergenic sequences between ORF8 and N (ACAAACTAAA), Venus (green), the PTV-1 2A (light blue), and the viral N (dark blue) are indicated. (*B*) Vero E6 cells were mock infected or infected with rBAC-SARS-CoV-2/WT or rSARS-CoV-2/Venus-2A for 48 h, fixed, and immunostained with a MAb against the viral N protein (1C7C7). Cell nuclei were stained with DAPI. Representative images are shown. (Scale bars, 100 μm.) (*C*) Whole cell lysates from Vero E6 cells mock infected or infected with rSARS-CoV-2 WT or Venus-2A for 48 h were subjected to Western blot analysis using antibodies against Venus and the viral N protein (1C7C7). β-actin was used as a loading control. (*D*) Total cellular RNA from Vero E6 cells mock infected or infected with WT or Venus-2A rSARS-CoV-2 was isolated at 48 hpi. RT-PCR was used to amplify Venus (*Top*) or the region between the ORF8 and N proteins (*Bottom*), and the products were separated on a 0.7% agarose gel.

Mice infected with rSARS-CoV-2/Δ7a-Venus succumbed to viral infection by 8 dpi, and mice infected with rSARS-CoV-2/Venus-2A or rSARS-CoV-2/WT succumbed to infection by 9 dpi (Fig. 3*H*).

In Vitro and In Vivo Stability of rSARS-CoV-2/Venus-2A. Because reporter-expressing rSARS-CoV-2 applications necessitate genetic and phenotypic stability, we evaluated the stability of rSARS-CoV-2/Venus-2A in vitro and in vivo. To that end, we passaged the rSARS-CoV-2/Venus-2A seven times in Vero E6 cells, and TCSs from selected passages were subjected to the analysis of plaque assay using a fluorescent imaging system and immunostaining with the 1C7C7 N protein monoclonal antibody (MAb) (Fig. 4 *A*, *Left*). Viruses present in TCS from P1, P3, P5, and P7 retained 100% Venus expression (Fig. 4 *A*, *Right*). For the in vivo stability evaluation of rSARS-CoV-2/Venus-2A, lung homogenates from K18 hACE2 transgenic mice at 1, 2, 4, and 6 dpi infected with rSARS-CoV-2/Venus-2A were subjected to plaque assay using a fluorescent imaging system and immunostaining with the 1C7C7 N protein MAb (Fig. 4 *B*, *Left*). Lung homogenates from 1 and 2 dpi retained 100% Venus expression, and homogenates from 4 and 6 dpi retained 99% and 98%, respectively, Venus expression (Fig. 4 *B*, *Right*).

Visualization of SARS-CoV-2 Replication Dynamic In Vivo. While fluorescent Venus expression allowed us to conduct ex vivo imaging of lungs from SARS-CoV-2–infected mice, it did not allow us to track viral infection in the entire mouse using IVIS. To circumvent this problem, we engineered an Nluc-expressing rSARS-CoV-2 using our reverse genetic system and the same 2A strategy (Fig. 5*A*). This rSARS-CoV-2/Nluc-2A exhibited a similar plaque phenotype and comparable growth kinetics in Vero E6 cells to the rSARS-CoV-2/WT and our previously described rSARS-CoV-2/Δ7a-Nluc (Fig. 5 *B* and *C*). Notably, Nluc expression levels were increased by more than 30-fold in Vero E6 cells infected with rSARS-CoV-2/Nluc-2A compared with cells infected with rSARS-CoV-2/Δ7a-Nluc at 72 hpi (Fig. 5*D*).

Since the rSARS-CoV-2/Nluc-2A expressed significantly higher levels of Nluc than those of our previously described rSARS-CoV-2/Δ7a-Nluc in vitro, we evaluated whether SARS-CoV-2 infection could be tracked in vivo using Nluc expression directed by rSARS-CoV-2/Nluc-2A. To that end, we infected (10^5 pfu) K18 hACE2 transgenic mice intranasally with rSARS-CoV-2/Nluc-2A or rSARS-CoV-2/WT (Fig. 6). Mice were anesthetized, retroorbitally injected with Nluc substrate, and then imaged under an IVIS at 1, 2, 4, and 6 dpi. Nluc expression was readily detected in mice infected with rSARS-CoV-2/Nluc-2A but not those infected with rSARS-CoV-2/WT (Fig. 6*A*), as previously shown in vitro (Fig. 5*D*). Quantitative analyses showed that Nluc intensity continued increasing at later dpi (Fig. 6*B*). Gross lesions on the lung surface of mice infected with rSARS-CoV-2/Nluc-2A were comparable to those in the WT rSARS-CoV-2–infected mice (Fig. 6 *C* and *D*). Importantly, viral titers detected in the rSARS-CoV-2/Nluc-2A–infected mice were comparable to those infected with rSARS-CoV-2/WT in all organs tested at different dpi (Fig. 6*E*), even though Nluc activity was only detected in the organs from rSARS-CoV-2/Nluc-2A–infected mice (Fig. 6*F*). Unexpectedly, the Nluc intensity did not correlate with the viral titers in the lungs at 4 and 6 dpi (Fig. 6*G*), indicating that Nluc accumulates in vivo.

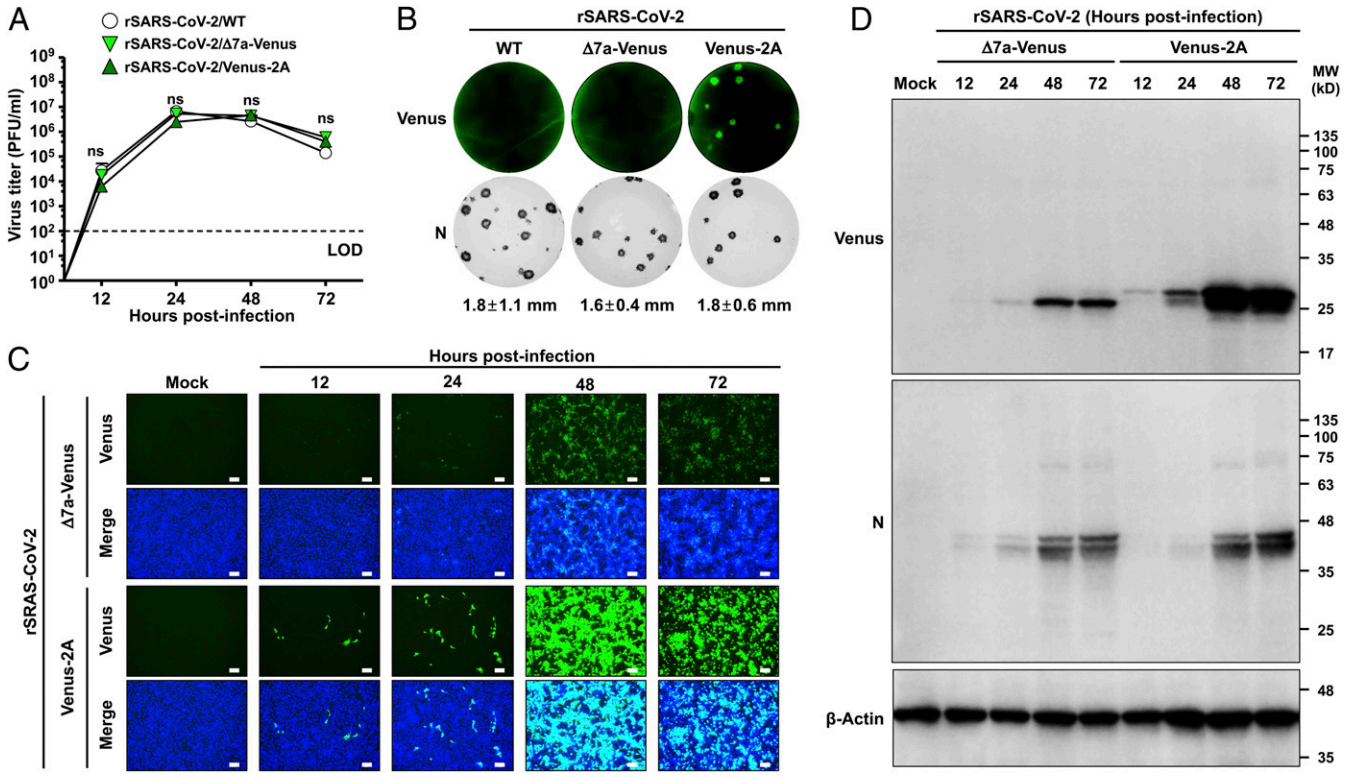

Fig. 2. Characterization of rSARS-CoV-2/Venus-2A in vitro. (*A*) TCSs from cells infected (MOI 0.01) with rSARS-CoV-2/WT, rSARS-CoV-2/Δ7a-Venus, or rSARS-CoV-2/Venus-2A were collected at the indicated times pi, and viral titers were determined by plaque assay. LOD, limitation of detection; ns, not significant. (*B*) Vero E6 cells infected with ~15 pfu of rSARS-CoV-2/WT (*Left*), rSARS-CoV-2/Δ7a-Venus (*Middle*), or rSARS-CoV-2/Venus-2A (*Right*) were fixed, and fluorescent plaques were photographed under a ChemiDoc MP imaging system (*Top*). After imaging, viral plaques were immunostained with the 1C7C7 N protein MAb (*Bottom*). (*C*) Vero E6 cells infected (MOI 0.001) with rSARS-CoV-2/Δ7a-Venus (*Top*) or rSARS-CoV-2/Venus-2A (*Bottom*) were monitored at the indicated times pi using fluorescent microscopy. Cell nuclei were stained with DAPI. (Scale bars, 100 μm.) (*D*) At the same times pi, whole cell lysate were prepared and analyzed by Western blot analysis using antibodies against Venus and SARS-CoV-2 N protein (1C7C7). β-Actin was used as a loading control.

Meanwhile, we also compared the pathogenicity of rSARS-CoV-2/Nluc-2A and rSARS-CoV-2/WT in K18 hACE2 transgenic mice. Both rSARS-CoV-2/Nluc-2A and rSARS-CoV-2/WT showed similar virulence (Fig. 6 *H* and *I*).

Effect of Neutralizing Abs on Progression of Nluc-2A Virus Infection In Vivo. Although several vaccines against COVID-19 have been already authorized for emergency use by US Food and Drug Administration (FDA), identification and characterization of SARS-CoV-2 neutralizing Abs (NAbs) represent a valuable therapeutic option to counteract the putative emergence of variants of concern (VoC). Currently, most NAb screenings are performed in tissue cultured cells rather than in vivo, which is heavily reliant upon viral titration of animal organs, a process that is time and labor intensive. We therefore investigated whether the use of rSARS-CoV-2/Nluc-2A could expedite the screening process and facilitate the investigation of how NAb affects the kinetics of virus infection. To that end, we treated K18 hACE2 transgenic mice prophylactically with 1212C2, a previously described SARS-CoV-2 NAb (22), for 12 h, and then infected them (10^5 pfu) with rSARS-CoV-2/Nluc-2A. Noninvasive longitudinal imaging of the mice revealed that 1212C2-treated mice dramatically restricted rSARS-CoV-2/Nluc-2A multiplication, since no significant Nluc signal was detected at any time point examined (Fig. 7 *A* and *B*). These results were also supported by the observation of reduced lung surface lesions (Fig. 7 *C* and *D*), Nluc expression (Fig. 7*E*), and virus titers (Fig. 7*F*) in the nasal turbinate, lungs, and brains of 1212C2-treated mice. Moreover, 1212C2 was able to protect mice from clinical symptoms of rSARS-CoV-2/Nluc-2A infection as determined by changes in body weight (Fig. 7*G*) and survival rate (Fig. 7*H*).

Discussion

In this study, we report a strategy to generate replication-competent reporter-expressing (e.g., Venus or Nluc) rSARS-CoV-2 using the well-documented BAC-based reverse genetic system (20). Our rSARS-CoV-2/Venus-2A and rSARS-CoV-2/Nluc-2A both exhibited rSARS-CoV-2/WT–like growth properties in vitro and in vivo without displaying attenuation and allowed us to monitor virus infection ex vivo in the lungs of infected mice (rSARS-CoV-2/Venus-2A) and the dynamic of viral replication in the entire mouse (rSARS-CoV-2/Nluc-2A) using noninvasive longitudinal in vivo imaging. Importantly, we demonstrate the feasibility of using rSARS-CoV-2/Nluc-2A to rapidly identify prophylactics and/or therapeutics in vivo.

We and others have previously demonstrated the feasibility of using this 2A approach to generate recombinant viruses expressing reporter genes fused to a viral protein (16–18, 23). To generate these novel reporter rSARS-CoV-2 expressing a higher level of reporter gene, we placed the PTV-1 2A self-cleaving peptide between the reporter gene and the viral N gene (Fig. 1). This results in the expression of a polyprotein that is posttranslationally cleaved at the 2A site leading to the individual expression of the reporter gene and the viral N protein (24), and the expression of Venus in rSARS-CoV-2/Venus-2A was extremely increased in vitro and in vivo (Figs. 2 and 3, respectively). The rationale of cloning the reporter gene fused to the viral N gene to increase reporter gene expression was based on

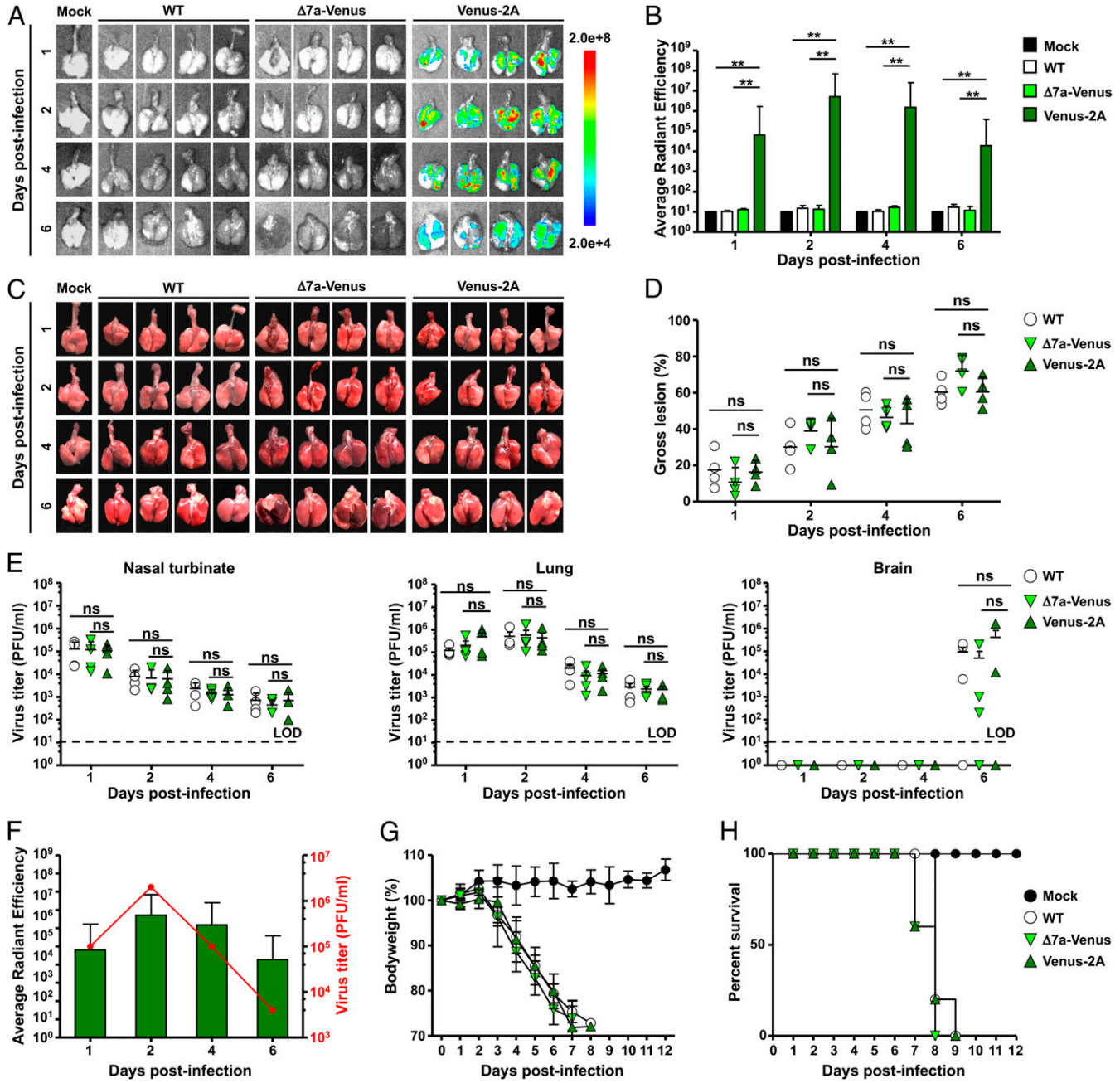

Fig. 3. Replication dynamic of rSARS-CoV-2/Venus-2A in vivo. (*A* and *B*) Five-week-old K18 hACE2 transgenic mice were mock infected or infected (10^5 pfu per mouse) with rSARS-CoV-2/WT (WT), rSARS-CoV-2/Δ7a-Venus (Δ7a-Venus), or rSARS-CoV-2/Venus-2A (Venus-2A). Lungs were excised at 1, 2, 4, and 6 dpi, and Venus expression was assessed under an IVIS (*A*). Fluorescence intensity was quantitively analyzed by the program of Aura (*B*). $^{**}P < 0.01$. (*C* and *D*) Images of lungs were photographed at 1, 2, 4, and 6 dpi (*C*), and the gross lesions on the lung surfaces were quantitively analyzed by ImageJ (*D*). (*E*) Viral titers in the nasal turbinate (*Left*), lungs (*Middle*), and brain (*Right*) were determined by plaque assay. (*F*) Correlation between viral titers and Venus intensity in the lungs of rSARS-CoV-2/Venus-2A infected mice. (*G* and *H*) Five-week-old K18 hACE2 transgenic mice were mock infected or intranasally inoculated with 10^5 pfu per mouse of rSARS-CoV-2/WT, rSARS-CoV-2/Δ7a-Venus, or rSARS-CoV-2/Venus-2A and monitored for 12 d for body weight loss (*G*) and survival (*H*).

the N protein being one of the most abundant structural proteins produced during SARS-CoV-2 and other CoVs infections (25–27). Importantly, this 2A approach does not remove any viral gene from the viral genome. Although recent data from our laboratory (28) suggest that ORF7a is not essential for SARS-CoV-2 replication in vitro and in vivo (29), it is still largely unknown whether the lack of ORF7a affects some unknown aspects of SARS-CoV-2 pathogenesis. In addition, this also increases the instability concern regarding the reporter gene, as shown in a recent study where a reporter gene fused into the C terminus of ORF7a was not stable (30). Contrarily, our rSARS-CoV-2/Venus-2A exhibited 100% stability after seven passages in cultured cells and retained 98% stability in vivo at 6 dpi (Fig. 4).

The increased expression level of reporter gene also facilitates the use of bioluminescence imaging of the entire infected mouse. The rSARS-CoV-2/Nluc-2A expressed ~30-fold higher levels of Nluc than rSARS-CoV-2/Δ7a-Nluc in cultured cells (Fig. 5),

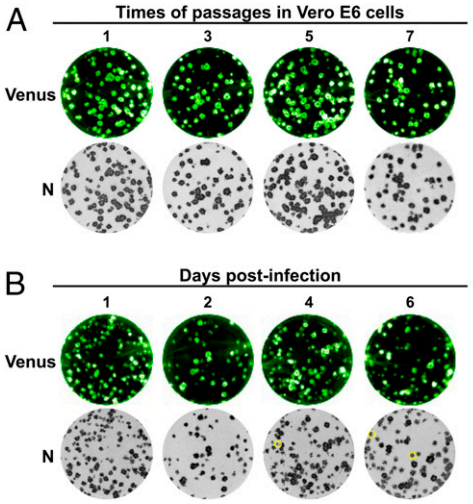

	P1	P3	P5	P7
Venus+	68	66	71	72
N+	68	66	71	72
Venus+/N+	100%	100%	100%	100%

	D1	D2	D4	D6
Venus+	78	52	98	108
N+	78	52	99	110
Venus+/N+	100%	100%	99%	98%

Fig. 4. Stability of rSARS-CoV-2/Venus-2A. (*A*) The rSARS-CoV-2/Venus-2A was passaged seven times in Vero E6 cells, and the first (P1), third (P3), fifth (P5), and seventh (P7) passage supernatants were analyzed by plaque assay. Fluorescent plaques were detected under a ChemiDoc MP imaging system (*Top Left*) and then were immunostained with the 1C7C7 N MAb (*Bottom Left*). The ratio of Venus-positive over N-positive plaques was calculated (*Right*). (*B*) The lung from one of the mice described in Fig. 3 was homogenized, and the clarified supernatant was collected and analyzed by plaque assay. Fluorescent plaques were detected using the ChemiDoc MP imaging system (*Top Left*) and then immunostained with the N protein MAb 1C7C7 N (*Bottom*). Venus-negative plaques were circled in yellow in *Bottom Left*. The ratio of Venus-positive over N-positive plaques was calculated (*Right*).

which allowed us to track the viral infection as early as 1 dpi (Fig. 6*A*). Another advantage is that the rSARS-CoV-2/Nluc-2A could provide real-time and longitudinal information in a non-invasive manner during infection rather than providing a static "snapshot" using the traditional necropsy and titration of tissues or organs from an infected animal. Notably, Nluc activity correlated well with the titers detected in the lungs at 1 and 2 dpi (Fig. 6 *E* and *F*). In contrast, viral titers in lungs were decreased

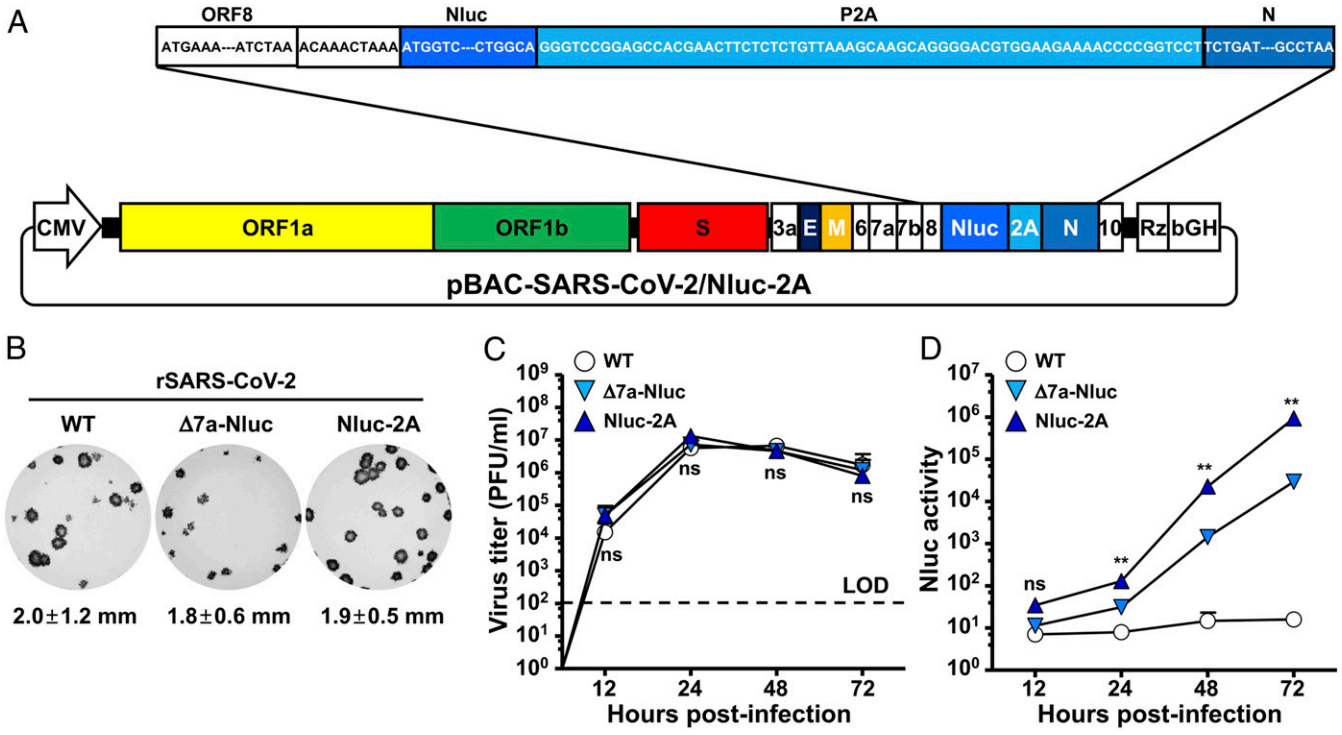

Fig. 5. Generation and characterization of rSARS-CoV-2 expressing Nano luciferase-2A in vitro. (*A*) Schematic representation of the BAC for generation of rSARS-CoV-2/Nluc-2A. The sequence encoding the fusion construct Nluc-2A was inserted in the viral genome of SARS-CoV-2 in the BAC. The viral ORF8, the intergenic sequences between ORF8 and N (ACAAACTAAA), Nluc (bright blue), the PTV-1 2A (light blue), and the viral N (dark blue) are indicated. (*B*) Vero E6 cells infected with ~15 pfu of rSARS-CoV-2/WT (*Left*), rSARS-CoV-2/Δ7a-Nluc (*Middle*), or rSARS-CoV-2/Nluc-2A (*Right*) were fixed, permeabilized, and immunostained with the 1C7C7 N protein MAb. (*C*) TCSs from Vero E6 cells infected (MOI 0.01) with rSARS-CoV-2/WT, rSARS-CoV-2/Δ7a-Nluc, or rSARS-CoV-2/Nluc-2A were collected at the indicated times pi, and TCSs were titrated by plaque assay. (*D*) TCSs from Vero E6 cells infected (MOI 0.01) with rSARS-CoV-2/WT, rSARS-CoV-2/Δ7a-Nluc, or rSARS-CoV-2/Nluc-2A were collected at the indicated times pi and Nluc activity in the TCSs was determined. $^{**}P < 0.01$.

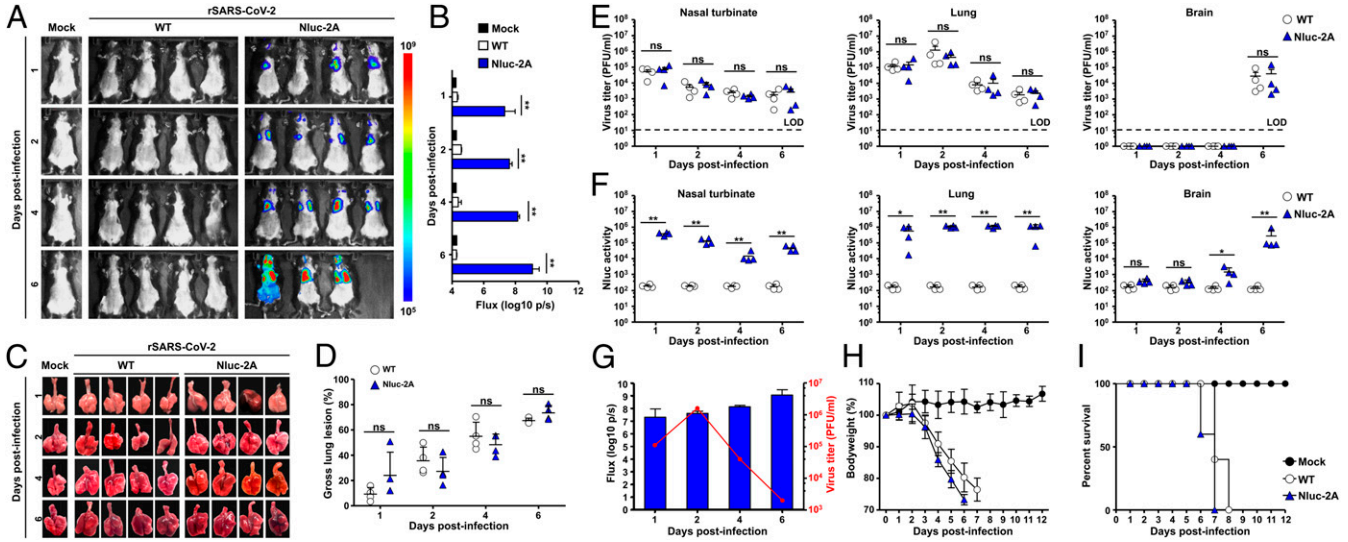

Fig. 6. In vivo dynamic of SARS-CoV-2 infection by real-time monitoring of Nluc expression. (*A* and *B*) Five-week-old K18 hACE2 transgenic mice were mock infected or infected (10^5 pfu per mouse) with rSARS-CoV-2/WT (WT) or rSARS-CoV-2/Nluc-2A (Nluc-2A). Mice were anesthetized at 1, 2, 4, and 6 dpi and retroorbitally injected with the Nluc substrate. Nluc expression was determined using an IVIS system (*A*) and quantitively analyzed by the Aura program (*B*). (*C* and *D*) Lungs were excised and photographed at 1, 2, 4, and 6 dpi (*C*), and gross lesions on the lung surfaces were quantitively analyzed by ImageJ (*D*). (*E*) Nluc activity in the nasal turbinate (*Left*), lungs (*Middle*), and brain (*Right*) from infected mice were determined using a multiplate reader. (*F*) Viral titers in the nasal turbinate (*Left*), lungs (*Middle*), and brain (*Right*) were determined by plaque assay. $^{**}P < 0.01$. (*G*) Correlation between viral titers and Nluc intensity in the lungs of rSARS-CoV-2/Nluc-2A–infected mice. (*H* and *I*) Five-week-old K18 hACE2 transgenic mice were mock infected or infected (10^5 pfu per mouse) with rSARS-CoV-2/WT or rSARS-CoV-2/Nluc-2A and monitored for 12 d for changes in body weight (*H*) and survival (*I*).

at 4 and 6 dpi, whereas we still detected high levels of Nluc activity. This may reflect Nluc stability (31), which can lead to the accumulation and gradual increase of Nluc signal during the course of viral infection. This explanation was also supported by the in vitro infection data in which the viral titers were declining and yet the Nluc activity was gradually increasing (Fig. 5*D*).

NAb represents a promising prophylactic and/or therapeutic treatment against SARS-CoV-2, particularly for individuals infected with newly identified VoC. However, evaluation of SARS-CoV-2 NAb in vivo relies on the necropsy and viral titration of tissues and/or organs from infected animals. To overcome this limitation, we established a rapid method based

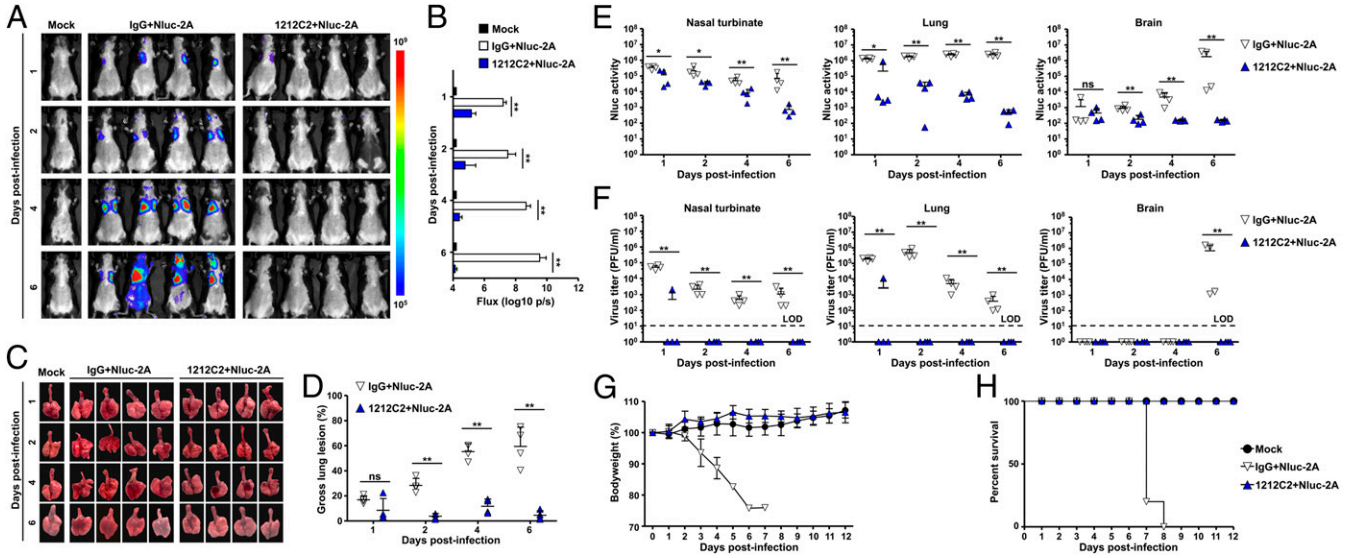

Fig. 7. Prophylactic effect of 1212C2 on mice infected with rSARS-CoV-2/Nluc-2A. (*A* and *B*) Five-week-old K18 hACE2 transgenic mice were injected with isotype IgG control or 1212C2 MAbs, and, 12 h after treatment, mice were infected (10^5 pfu per mouse) with rSARS-CoV-2/Nluc-2A (Nluc-2A). Mock-treated and mock-infected mice were included as controls. Mice were anesthetized at 1, 2, 4, and 6 dpi and retroorbitally injected with the Nluc substrate. Nluc expression was determined using an IVIS system (*A*) and quantitively analyzed by the Aura program (*B*). $^{**}P < 0.01$. (*C* and *D*) The lungs were excised and photographed at 1, 2, 4, and 6 dpi (*C*), and the gross lesions on the lung surfaces were quantitively analyzed by ImageJ (*D*). $^{**}P < 0.01$. (*E*) Nluc activity in the nasal turbinate (*Left*), lungs (*Middle*), and brains (*Right*) from infected mice were measured using a multiplate reader. $^{*}P < 0.05$; $^{**}P < 0.01$. (*F*) Viral titers in the nasal turbinate (*Left*), lungs (*Middle*), and brain (*Right*) were determined by plaque assay. $^{**}P < 0.01$. (*G* and *H*) Five-week-old K18 hACE2 transgenic mice were injected with isotype IgG control or 1212C2 MAbs, and, 12 h after treatment, mice were infected (10^5 pfu per mouse) with rSARS-CoV-2/Nluc-2A (Nluc-2A). Mock-treated and mock-infected mice were included as controls. Mice were monitored for 12 d for changes in body weight (*G*) and survival (*H*).

on a noninvasive measurement of Nluc expression. By using this IVIS, NAbs could be easily identified as early as 1 dpi and in a relatively high-throughput method. This was further supported by Nluc activity, viral titration, body weight changes, and survival rate (Fig. 7), indicating our strategy provides a rapid in vivo screening method to identify NAbs against SARS-CoV-2.

In the present work, we have documented a strategy to generate replication-competent reporter rSARS-CoV-2 expressing higher levels of reporter gene than those previously described, by substituting the viral ORF7a protein with the report gene. This strategy does not eliminate any viral gene, and these reporter-expressing rSARS-CoV-2 were genetically stable and replicated as efficiently as rSARS-CoV-2/WT both in vitro and in vivo, with comparable pathogenicity in K18 hACE2 transgenic mice. Notably, the robust levels of reporter gene expression of these reporter-expressing rSARS-CoV-2 represent an excellent option to study viral pathogenesis, tissue tropism, and replication kinetics of SARS-CoV-2, including recently identified VoC.

Materials and Methods

Biosafety. All the in vitro and in vivo experiments with infectious rSARS-CoV-2 were conducted in appropriate biosafety level (BSL) 3 and animal BSL3 (ABSL3) laboratories, respectively, at Texas Biomedical Research Institute (Texas Biomed). Experiments were approved by the Texas Biomed Institutional Biosafety and Animal Care and Use (IACUC) committees.

Cells and Viruses. African green monkey kidney epithelial cells (Vero E6, CRL-1586) were obtained from the American Type Culture Collection and maintained in Dulbecco's modified Eagle medium (DMEM) supplemented with 5% (vol/vol) fetal bovine serum (FBS, VWR) and 1% penicillin–streptomycin–glutamine (PSG) solution (Corning).

The rSARS-CoV-2 were generated based on the backbone of the USA-WA1/2020 strain using a previously described BAC-based reverse genetics system (19, 20).

Rescue of rSARS-CoV-2. Virus rescue experiments were performed as previously described (32). Briefly, confluent monolayers of Vero E6 cells (10^6 cells per well, six-well plates, triplicates) were transfected with 4.0 μg per well of SARS-CoV-2 BAC using Lipofectamine 2000. After 24 h, transfection media was exchanged for postinfection media (DMEM supplemented with 2% FBS and 1% PSG), and cells were split and seeded into T75 flasks 72 h post-transfection. After incubation for another 72 h, TCSs were collected, labeled as P0, and stored at −80 °C. After being titrated, the P0 virus was used to infect fresh Vero E6 cells at MOI 0.0001 for 72 h to generate P1 stocks. P1 viral stocks were aliquoted and stored at −80 °C until being used.

Western Blot. Whole cell lysates, sodium dodecyl sulfate polyacrylamide gel electrophoresis (SDS-PAGE), and Western blotting were performed as previously described (16). Briefly, cells were lysed in passive lysis buffer (Promega) at 4 °C for 30 min, followed by centrifugation at 12,000 × *g* at 4 °C for another 30 min. Equivalent amounts of cell lysates were subjected to 12% SDS-PAGE and transferred to nitrocellulose membranes. After blocking with 5% bovine serum albumin in PBS containing 0.1% Tween 20 at room temperature for 1 h, the membranes were incubated with the indicated primary antibodies at 4 °C overnight, followed by horseradish peroxidase-conjugated secondary antibody incubation at 37 °C for 1 h. β-Actin was used as the loading control. Membranes were developed with ECL detection reagent (Thermo Fisher Scientific) in the ChemiDoc MP Imaging System (Bio-Rad).

Immunofluorescence Assay. Vero E6 cells (10^6 cells per well, six-well plate format, triplicates) were mock inoculated or inoculated with the TCS (1 mL per well) of Vero E6 cells transfected with the BACs collected at 72 h post-transfection. At 48 h postinoculation, cells were fixed with 10% formaldehyde solution at 4 °C overnight and permeabilized using 0.5% (vol/vol) Triton X-100 in PBS for 15 min at room temperature. Then, cells were incubated overnight with 1 μg/mL of a SARS-CoV cross-reactive N MAb (1C7C7) at 4 °C, washed stringently with PBS, and stained with a fluorescein isothiocyanate–labeled goat anti-mouse IgG (1:200). Finally, cells were visualized and imaged under an EVOS fluorescent microscope (Thermo Fisher Scientific).

RT-PCR. Total RNA from virus-infected (MOI 0.01) Vero E6 cells (10^6 cells per well, six-well plate format) was extracted with TRIzol Reagent (Thermo Fisher Scientific) according to the manufacturer's instructions. RT-PCR amplification of the viral genome spanning nucleotides 27,895 to 29,534 (according to the SARS-CoV-2 USA-WA1/2020 viral genome) was performed using Super Script II Reverse transcriptase (Thermo Fisher Scientific) and Expanded High Fidelity PCR System (Sigma Aldrich). The amplified DNA products were separated on 0.7% agarose gel.

Plaque Assay and Immunostaining. Confluent monolayers of Vero E6 cells (10^6 cells per well, six-well plate format, triplicates) were infected with serial viral dilutions for 1 h at 37 °C. After viral adsorption, cells were overlaid with pi media containing 1% low melting agar and incubated at 37 °C. At 72 hpi, cells were fixed overnight with 10% formaldehyde solution. For visualization of Venus, plates were photographed under a ChemiDoc MP Imaging System. For immunostaining, cells were permeabilized with 0.5% (vol/vol) Triton X-100 in PBS for 15 min at room temperature and immunostained using the SARS-CoV cross-reactive N protein 1C7C7 MAb (1 μg/mL) and the Vectastain ABC kit (Vector Laboratories), following the manufacturers' instruction. After immunostaining, plates were scanned and photographed using a ChemiDoc MP Imaging System.

Virus Growth Kinetics. Confluent monolayers of Vero E6 cells (six-well format, 10^6 cells per well, triplicates) were mock infected or infected (MOI 0.01) with rSARS-CoV-2/WT, rSARS-CoV-2/Δ7a-Venus, rSARS-CoV-2/Venus-2A, or rSARS-CoV-2/Nluc-2A. After 1 h of virus adsorption at 37 °C, cells were washed with chilled PBS and overlaid with 3 mL of pi medium and incubated at 37 °C. At the indicated times (12, 24, 48, and 72 hpi), viral titers in the TCSs were determined by plaque assay (33). Presence of Nluc in the TCSs from mock and rSARS-CoV-2/WT–, rSARS-CoV-2/Δ7a-Nluc–, or rSARS-CoV-2/Nluc-2A–infected cells was quantified using Nano-Glo Luciferase Assay System (Promega) following the manufacturers' specification.

Animal Experiments. All animal protocols were approved by Texas Biomed IACUC (1718MU). Five-week-old female K18 hACE2 transgenic mice were purchased from The Jackson Laboratory and maintained in the animal facility at Texas Biomed under specific pathogen-free conditions. For virus infection, mice were anesthetized following gaseous sedation in an isoflurane chamber and inoculated intranasally with a dose of 10^5 pfu per mouse.

For ex vivo imaging of lungs, mice were humanely killed at 1, 2, 4, and 6 dpi to collect lungs. Fluorescent images of lungs were photographed using an IVIS (AMI HTX), and the brightfield images of lungs were taken using an iPhone 6s (Apple). Nasal turbinate, lungs, and brains from mock or infected animals were homogenized in 1 mL of PBS for 20 s at 7,000 rpm using a Precellys tissue homogenizer (Bertin Instruments). Tissue homogenates were centrifuged at 12,000 × *g* (4 °C) for 5 min, and supernatants were collected and titrated by plaque assay and immunostaining as previously described.

For in vivo bioluminescence imaging, mice were anesthetized with isoflurane, injected retroorbitally with 100 μL of Nano-Glo luciferase substrate (Promega), and immediately imaged. The bioluminescence data acquisition and analysis were performed using the Aura program (AMI spectrum). Flux measurements were acquired from the region of interest. The scale used is included in each figure. Immediately after imaging, nasal turbinate, lungs, and brains were collected and homogenized in 1 mL of PBS. Supernatants were collected, and presence of virus was determined by plaque assay and immunostaining, as described above. Nluc activity in the TCSs was determined under a multiplate reader (BioTek Instruments, Inc.) as above.

For the body weight and survival studies, 5-week-old female K18 hACE2 transgenic mice were infected intranasally with 10^5 pfu per animal following gaseous sedation in an isoflurane chamber. After infection, mice were monitored daily for morbidity (body weight) and mortality (survival rate) for 12 d. Mice showing a loss of more than 25% of their initial body weight were defined as reaching the experimental end point and humanely killed, and the survival curves were plotted according to the method of Kaplan–Meier (34).

Statistical Analysis. All data are presented as mean ± SD for each group and analyzed by SPSS13.0 (IBM). A P value of less than 0.05 ($P < 0.05$) was considered statistically significant.

Data Availability. All study data are included in the article. All primer sequences used for RT-PCR are available upon request. The plasmids described in this study are available at the following website: https://www.txbiomed.org/services-2/reverse-genetics-plasmids.

ACKNOWLEDGMENTS. We thank Dr. Thomas Moran at The Icahn School of Medicine at Mount Sinai for providing the SARS-CoV cross-reactive 1C7C7 N protein MAb.

1. B. Hu, H. Guo, P. Zhou, Z.-L. Shi, Characteristics of SARS-CoV-2 and COVID-19. *Nat. Rev. Microbiol.* **19**, 141–154 (2021).
2. E. de Wit, N. van Doremalen, D. Falzarano, V. J. Munster, SARS and MERS: Recent insights into emerging coronaviruses. *Nat. Rev. Microbiol.* **14**, 523–534 (2016).
3. J. T. Wu, K. Leung, G. M. Leung, Nowcasting and forecasting the potential domestic and international spread of the 2019-nCoV outbreak originating in Wuhan, China: A modelling study. *Lancet* **395**, 689–697 (2020).
4. R. Lu *et al*., Genomic characterisation and epidemiology of 2019 novel coronavirus: Implications for virus origins and receptor binding. *Lancet* **395**, 565–574 (2020).
5. Z. Xu *et al*., Pathological findings of COVID-19 associated with acute respiratory distress syndrome. *Lancet Respir. Med.* **8**, 420–422 (2020).
6. J. Li *et al*., Clinical features of familial clustering in patients infected with 2019 novel coronavirus in Wuhan, China. *Virus Res.* **286**, 198043 (2020).
7. M. Imai *et al*., Syrian hamsters as a small animal model for SARS-CoV-2 infection and countermeasure development. *Proc. Natl. Acad. Sci. U.S.A.* **117**, 16587–16595 (2020).
8. F. S. Oladunni *et al*., Lethality of SARS-CoV-2 infection in K18 human angiotensin-converting enzyme 2 transgenic mice. *Nat. Commun.* **11**, 6122 (2020).
9. S. H. Sun *et al*., A mouse model of SARS-CoV-2 infection and pathogenesis. *Cell Host Microbe* **28**, 124–133.e4 (2020).
10. D. K. Singh *et al*., Responses to acute infection with SARS-CoV-2 in the lungs of rhesus macaques, baboons and marmosets. *Nat. Microbiol.* **6**, 73–86 (2021).
11. Y. I. Kim *et al*., Infection and rapid transmission of SARS-CoV-2 in ferrets. *Cell Host Microbe* **27**, 704–709.e2 (2020).
12. X. Xie *et al*., An infectious cDNA clone of SARS-CoV-2. *Cell Host Microbe* **27**, 841–848.e3 (2020).
13. K. Chiem *et al*., Generation and characterization of recombinant SARS-CoV-2 expressing reporter genes. *J. Virol.* **95**, e02209-20 (2021).
14. A. C. Sims *et al*., Severe acute respiratory syndrome coronavirus infection of human ciliated airway epithelia: Role of ciliated cells in viral spread in the conducting airways of the lungs. *J. Virol.* **79**, 15511–15524 (2005).
15. X. Xie *et al*., A nanoluciferase SARS-CoV-2 for rapid neutralization testing and screening of anti-infective drugs for COVID-19. *Nat. Commun.* **11**, 5214 (2020).
16. C. Ye, J. C. de la Torre, L. Martínez-Sobrido, Development of reverse genetics for the prototype New World mammarenavirus Tacaribe virus. *J. Virol.* **94**, e01014-20 (2020).
17. A. Nogales *et al*., A novel fluorescent and bioluminescent bireporter influenza A virus to evaluate viral infections. *J. Virol.* **93**, e00032-19 (2019).
18. Y. Cai *et al*., Recombinant Lassa virus expressing green fluorescent protein as a tool for high-throughput drug screens and neutralizing antibody assays. *Viruses* **10**, 655 (2018).
19. K. Chiem, C. Ye, L. Martinez-Sobrido, Generation of recombinant SARS-CoV-2 using a bacterial artificial chromosome. *Curr. Protoc. Microbiol.* **59**, e126 (2020).
20. C. Ye *et al*., Rescue of SARS-CoV-2 from a single bacterial artificial chromosome. *MBio* **11**, e02168-20 (2020).
21. J. Zheng *et al*., COVID-19 treatments and pathogenesis including anosmia in K18-hACE2 mice. *Nature* **589**, 603–607 (2021).
22. M. S. Piepenbrink *et al*., Therapeutic activity of an inhaled potent SARS-CoV-2 neutralizing human monoclonal antibody in hamsters. *Cell Rep. Med.* **2**, 100218 (2021).
23. B. Manicassamy *et al*., Analysis of in vivo dynamics of influenza virus infection in mice using a GFP reporter virus. *Proc. Natl. Acad. Sci. U.S.A.* **107**, 11531–11536 (2010).
24. G. Luke, H. Escuin, P. De Felipe, M. Ryan, 2A to the fore – Research, technology and applications. *Biotechnol. Genet. Eng. Rev.* **26**, 223–260 (2010).
25. J. A. Hiscox, D. Cavanagh, P. Britton, Quantification of individual subgenomic mRNA species during replication of the coronavirus transmissible gastroenteritis virus. *Virus Res.* **36**, 119–130 (1995).
26. Y. J. Hou *et al*., SARS-CoV-2 reverse genetics reveals a variable infection gradient in the respiratory tract. *Cell* **182**, 429–446.e14 (2020).
27. T. Scobey *et al*., Reverse genetics with a full-length infectious cDNA of the Middle East respiratory syndrome coronavirus. *Proc. Natl. Acad. Sci. U.S.A.* **110**, 16157–16162 (2013).
28. J. Silvas *et al*., Contribution of SARS-CoV-2 accessory proteins to viral pathogenicity in K18 hACE2 transgenic mice. *J. Virol.* **95**, e0040221 (2021).
29. A. Addetia *et al*., Identification of multiple large deletions in ORF7a resulting in in-frame gene fusions in clinical SARS-CoV-2 isolates. *J. Clin. Virol.* **129**, 104523 (2020).
30. S. J. Rihn *et al*., A plasmid DNA-launched SARS-CoV-2 reverse genetics system and coronavirus toolkit for COVID-19 research. *PLoS Biol.* **19**, e3001091 (2021).
31. M. P. Hall *et al*., Engineered luciferase reporter from a deep sea shrimp utilizing a novel imidazopyrazinone substrate. *ACS Chem. Biol.* **7**, 1848–1857 (2012).
32. G. Ávila-Pérez, J. G. Park, A. Nogales, F. Almazán, L. Martínez-Sobrido, Rescue of recombinant Zika virus from a bacterial artificial chromosome cDNA clone. *J. Vis. Exp.* **148**, e59537 (2019).
33. A. Nogales *et al*., Influenza A virus attenuation by codon deoptimization of the NS gene for vaccine development. *J. Virol.* **88**, 10525–10540 (2014).
34. B. Efron, Logistic-regression, survival analysis, and the Kaplan–Meier curve. *J. Am. Stat. Assoc.* **83**, 414–425 (1988).